Journal of Casting & Materials Engineering Vol. 10 No. 2 (2026) 42–53
https://doi.org/10.7494/jcme.2026.10.2.42

Numerical Optimisation of Investment-Cast Wheel Components for Drone Applications Using MAGMASOFT®

Joshua Samuel Isaac Jonthala[a*], **Janusz Lelito**[b]

[a]Foundry Institute, Technische Universität Bergakademie Freiberg, Bernhard-von-Cotta-Str. 4, 09599 Freiberg, Germany
[b]AGH University of Krakow, Faculty of Foundry Engineering, 23 Reymonta St., 30 059 Krakow, Poland
[*]*e-mail: joshua-samuel-isaac.jonthala@student.tu-freiberg.de*

Received: 11 April 2026/Accepted: 26 May 2026/Published online: 18 June 2026
This article is published with open access at AGH University of Krakow Journals

Abstract

Investment casting technology of thin-walled components for drone applications requires precise filling and solidification control to minimise porosity and ensure structural integrity. Porosity is one of the most common defects found in castings, and its prediction and analysis are essential for improving the quality of complex superalloy components. In this work, porosity-related defects were examined using the MAGMASOFT® 6.1 numerical simulation software for casting, focusing on the filling and solidification behaviour of an investment casting wheel body component in drone applications. A series of simulations were performed, and two design and simulation versions were developed, analysed and compared.

The wheel body component selected for this work is made of IN713 superalloy. The numerical modelling included the assessment of porosity distribution, hot spot formation, filling behaviour, cooling, and solidification patterns. Fifteen combinations of alloy and shell initial temperatures were evaluated to determine the most favourable thermal conditions for reducing porosity, considering the specific geometry and casting characteristics of the wheel. Based on the initial results, the casting design was modified by adjusting the runner geometry and assembly configuration.

This study introduces a two-stage simulation approach to optimise porosity reduction. The second version of the simulations demonstrated a noticeable reduction in pores, particularly in critical regions of the wheel body. The findings can support drone component manufacturers in improving casting reliability. The results confirm that simulation-driven optimisation of the casting design and thermal parameters can significantly improve the quality of the components produced by investment casting technology.

Keywords:
thin-walled casting, investment casting, numerical simulation, IN713 superalloy, shrinkage porosity, solidification

1. INTRODUCTION

Investment casting, also known as lost-wax casting, is a precision manufacturing technology widely used for producing small castings and geometrically complex components with high dimensional accuracy. The investment casting process allows it to produce extremely thin wall thicknesses. The limits that are generally quoted are, for steels, a minimum wall thickness of 1.5 mm and for light alloys 1 mm, subject to design acceptability. The production of these very thin wall thicknesses is greatly assisted by the elevated initial mould temperatures during casting and, of course, by the *vacuum casting* techniques now employed on an increasing scale [1].

The process begins with the fabrication of a wax pattern that replicates the final geometry of the component. These patterns may be produced through traditional tooling or increasingly through additive manufacturing, which enables rapid prototyping and the creation of intricate internal features.

The wax assembly is repeatedly coated in a ceramic slurry and refractory material to build a robust shell capable of withstanding high casting temperatures. Automated shellbuilding systems are often employed to ensure a uniform coating thickness and consistent mechanical properties of the mould. After curing, the assembly undergoes dewaxing, typically through steam autoclaving or flashfire methods, leaving a hollow ceramic mould. Preheating the mould removes residual moisture and reduces thermal stresses during metal pouring.

Casting is performed under a vacuum to prevent oxidation and minimise gas porosity in the molten superalloy. This controlled environment is essential for producing components with the mechanical integrity required for high-temperature applications. Once the alloy solidifies, the ceramic shell is removed, and the casting undergoes finishing operations such as trimming, machining, and heat treatment. Post-cast heat treatments are critical for nickel-based superalloys, as they promote microstructural homogenisation and enhance creep resistance, strength, and oxidation performance [2]. The main stages of the investment casting process are illustrated in Figure 1.

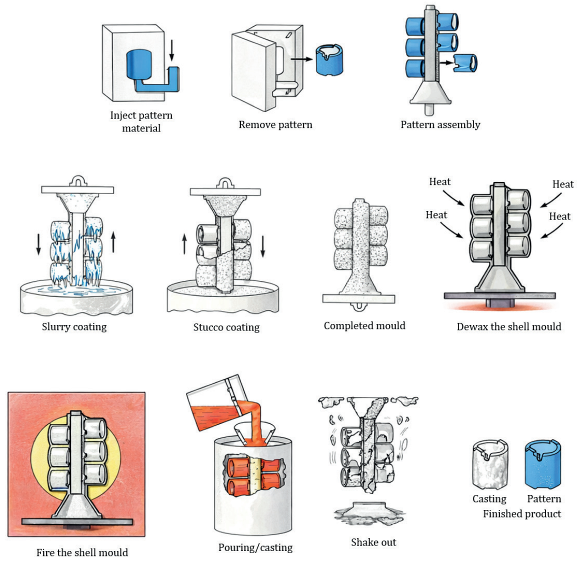

Fig. 1. Basic steps involved in investment casting [3]

Nickel-based superalloys such as IN713 are widely used in high-temperature aerospace components because of their excellent strength, corrosion resistance, and thermal stability [4, 5]. Like other cast Ni-base alloys, IN713 derives its mechanical performance from a γ/γ′ microstructure, where the γ′ ($Ni_3(Al, Ti)$-based phase provides high strength at elevated temperatures. Sims' foundational work established the importance of γ′ strengthening and solid-solution elements in defining the creep and oxidation resistance of cast superalloys, including IN713 [4].

Recent studies on IN713C confirm these microstructural–mechanical property relationships. Moreira et al. reported that as-cast IN713C exhibits a dendritic solidification structure with inter-dendritic segregation and carbide formation, features that strongly influence tensile strength, hardness, and high-temperature performance [6]. These microstructural characteristics are typical of cast Ni-based superalloys and highlight the sensitivity of IN713C to solidification conditions. The typical microstructure of as-cast IN713C is depicted in Figure 2.

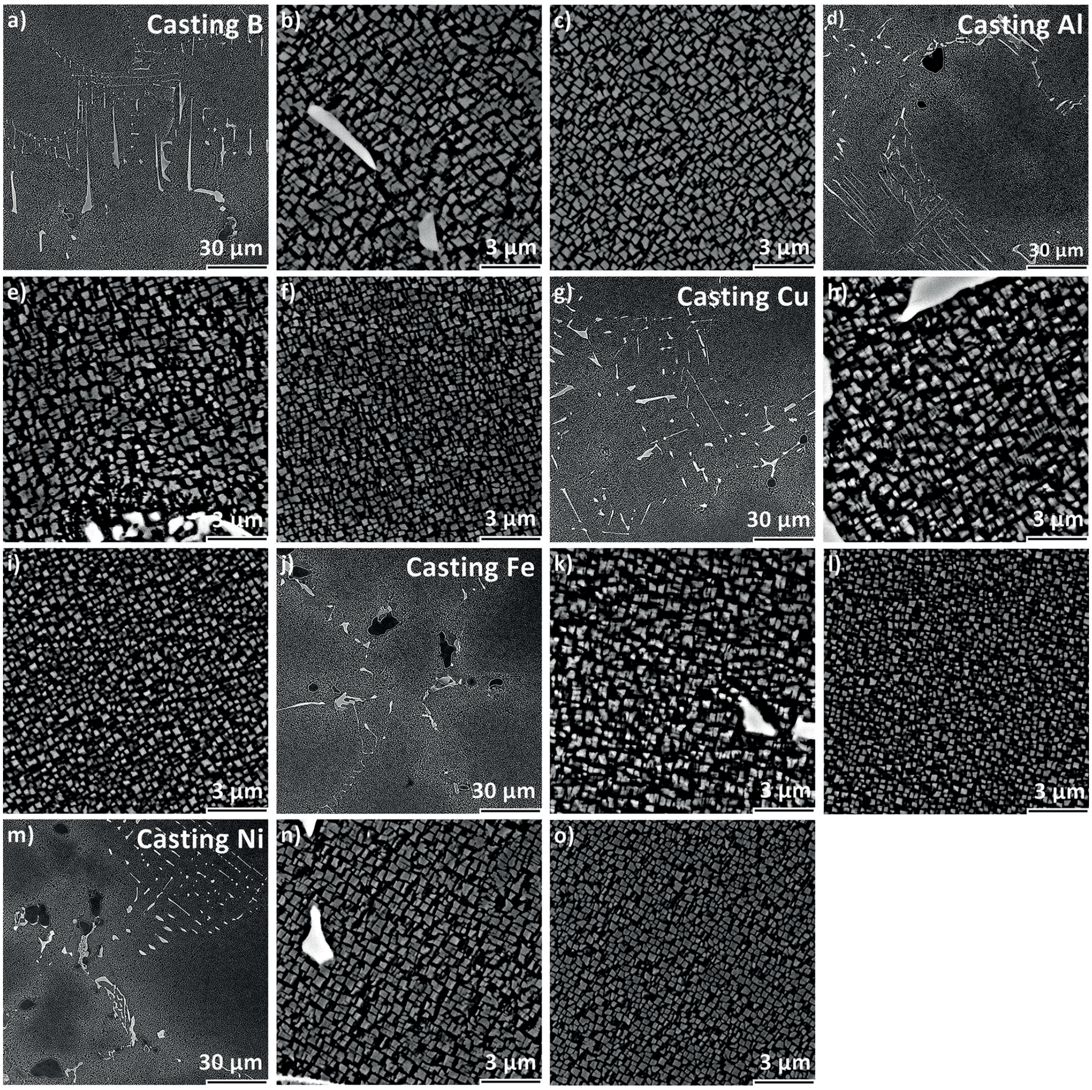

Fig. 2. Microstructure of Inconel 713C castings: (a, d, g, j, m) inter-dendritic spaces; (b, e, h, k, n) γ′ in inter-dendritic space; (c, f, i, l, o) γ′ precipitates in dendrite arm [7]

In investment casting, IN713 benefits from the ability to form complex geometries but remains sensitive to shrinkage porosity and segregation due to its high γ' content and solidification temperature. Achieving optimal mechanical performance therefore depends on controlled solidification and appropriate ceramic shell systems. The chemical composition of the IN713 alloy used in this study is presented in Table 1.

Table 1
Chemical composition of alloy IN713 [7]

Element	Typical content [%]	Function in alloy
Nickel (Ni)	~74	Base element
Chromium (Cr)	12–14	Oxidation and corrosion resistance
Molybdenum (Mo)	4–5	Solidsolution strengthening
Aluminium (Al)	5.5–6.5	γ' (Ni_3Al,) formation for precipitation hardening
Titanium (Ti)	0.5–1.0	Additional γ' strengthening
Carbon (C)	0.08–0.16	Carbide formation for creep resistance
Boron (B)	0.008–0.020	Grainboundary strengthening

High- or medium-density alumina (Al_2O_3) ceramic shells are widely used in investment casting because of their excellent thermal stability and chemical inertness at the high temperatures required for processing nickel-based superalloys. Alumina shells exhibit low reactivity with molten alloys, which helps minimise interfacial reactions and surface defects during casting. Varfolomeev and Shcherbakova demonstrated that Al_2O_3–Al_2O_3 shell systems maintain good chemical compatibility with nickel-based superalloys, reducing the formation of reaction layers at the mould-metal interface and improving the surface quality of the final casting [8].

The performance of alumina shells depends strongly on their density, slurry formulation, and stucco selection. Optimising these parameters enhances shell strength, permeability, and thermal shock resistance; properties essential for preventing cracking during dewaxing and metal pouring. Dave and Kaila emphasised that careful selection and optimisation of ceramic shell materials, including alumina-based systems, significantly improves mould integrity and casting reliability in industrial investment-casting operations [9].

Simulation is the imitation of the operation of a real-world process or system over time. Whether done by hand or on a computer, simulation involves the generation of an artificial history of a system and the observation of that artificial history to draw inferences concerning the operating characteristics of the real system that is represented [10]. In modern foundry practice, casting simulation has become an essential tool, enabling virtual prototyping of mould filling, solidification, defect prediction, etc. This significantly reduces development time and cost by minimising trial-and-error iterations and improving process reliability. Numerous studies have shown that simulation helps identify potential defects such as shrinkage porosity, misruns, or hot spots before physical production, thereby improving casting quality and increasing yield [3, 11–13]. The general workflow of the casting simulation process implemented in MAGMASOFT® is illustrated in Figure 3.

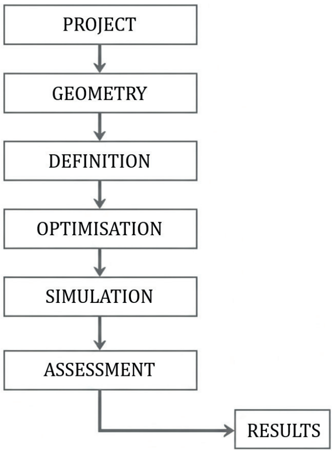

Fig. 3. MAGMASOFT® casting simulation process flow chart

For this study, the investment-casting simulations were performed using MAGMASOFT®, a commercial casting-process simulation piece of software widely used in industry and research. The numerical calculations were carried out at the Faculty of Foundry Engineering at AGH University of Krakow. MAGMASOFT® includes a dedicated Investment Casting module that models mould filling, solidification, defect (porosity) prediction, etc. The software employs a Finite Volume Method (FVM) to discretise the computational domain and solve the governing heat-transfer and fluid-flow equations.

Accurate numerical modelling requires the definition of uniqueness conditions:

- geometric conditions: describing the shape, dimensions, and topology of the casting, shell, and gating system;
- physical conditions: specifying thermophysical and physicochemical properties of alloys and ceramic materials;
- initial conditions: defining the temperature distribution and state of the system at the start of filling values;
- boundary conditions: describing interactions between casting, mould, and environment, including heat-transfer coefficients, inlet, hot topping, sand permeability, convection, and radiation.

These conditions collectively determine the fidelity of the simulation and its ability to predict real casting behaviour during solidification. As highlighted by Sabau and others, the accuracy of investmentcasting simulation depends strongly on the correct representation of interfacial heat transfer, mould properties, and radiative heat exchange [14].

The cooling of an investment casting is governed primarily by the total heat loss from the ceramic shell through thermal radiation and convection. Because investment cast components often have large, complex surface areas, accurately resolving radiative exchange across the entire shell can be computationally expensive. To address this, commercial simulation tools such as MAGMASOFT® implement specialised radiation algorithms that reduce computation time while maintaining acceptable accuracy for industrial casting simulations [15].

Thermal convection refers to the transport of heat within fluids (liquids and gases) that involves not only the transfer of energy but also the movement of the material itself and its accompanying heat content. This convection becomes relevant to investment casting when cooling media such as air circulate around the mould to extract heat from the system.

There are two types of convection:

1) forced convection: driven by external means such as fans or directed airflow, enhancing heat removal from the mould surface;
2) natural (free) convection: driven by buoyancy forces caused by temperature-induced density differences in the surrounding air.

The convective heat flux is described by *Newton's Law of Cooling* [16]**:**

$$q = -hA(T_s - T_f) \tag{1}$$

where:

q – heat flux [W] perpendicular to the surface area A [m^2],
h – convection heat transfer coefficient [W/(m$^2 \cdot$ K)],
T_s – surface temperature of the casting or mould [K],
T_f – temperature of the cooling fluid [K].

Thermal radiation: Thermal radiation is the transfer of energy by electromagnetic waves and does not require a medium, making it especially important in high-temperature or vacuum investment-casting environments. During the early stages of cooling and solidification, radiative heat transfer often dominates because ceramic shells have high emissivity and molten metals radiate strongly at elevated temperatures.

The radiative heat transfer rate is described by the *Stefan–Boltzmann Law* [16]. In the present study, emissivity is included implicitly through the material properties defined in the MAGMASOFT® database; therefore, it is not explicitly varied in the analytical formulation.

$$q = \varepsilon \sigma A T^4 \tag{2}$$

where:

q – radiative heat transfer rate [W],
ε – emissivity of the material [–] (for a black body $\varepsilon = 1$, while for real materials $\varepsilon < 1$),
σ – Stefan-Boltzmann constant [$5.669 \cdot 10^{-8}$ W/ (m$^2 \cdot$ K^4)],
A – radiating surface area [m^2],
T – absolute temperature [K].

In the present work, a constant metal–mould interfacial heat transfer coefficient (HTC) was applied at the casting–shell interface [16]:

$$h = \frac{q}{T_s - T_a} \tag{3}$$

where:

h – heat transfer coefficient [W/ (m$^2 \cdot$ K)],
q – amount of heat transfer [W/m^2],
T_s – surface temperature [K],
T_a – temperature of the surrounding fluid [K].

This value represents a typical order of magnitude for good metal-ceramic contact during the early stages of solidification. However, it does not account for the time-dependent decrease in HTC associated with gap formation and mould expansion, as discussed by Sabau in numerical studies of investment casting. Consequently, the predicted cooling rates and solidification times should be interpreted as an approximation rather than an exact reproduction of experimental conditions [14].

2. MATERIALS AND METHODS

2.1. Component geometry and initial design

The component analysed in this study is a wheel body intended for drone propulsion systems. The geometry was created in SOLIDWORKS, incorporating thin blades and a central hub to replicate the aerodynamic and structural requirements of drone applications. A straight central runner was designed and connected to the wheel body to form the initial casting configuration (Figs. 4 and 5).

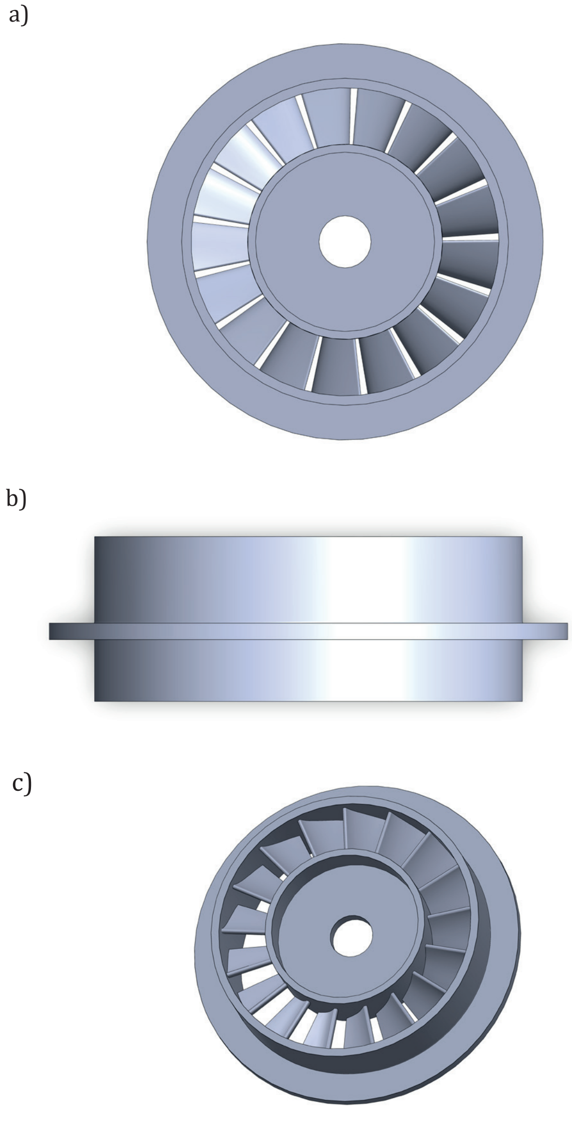

Fig. 4. CAD model of the investment-cast wheel component developed in SOLIDWORKS: a) top view; b) front view; c) isometric view

For investment casting, the wheel was assembled into a single-part tree structure. The complete geometry was exported as an STL file and imported into MAGMASOFT® for numerical simulation. Within the simulation environment, a pouring basin and hot topping were added, and material assignments were defined for the alloy, ceramic shell, and feeding system (Figs. 5 and 6).

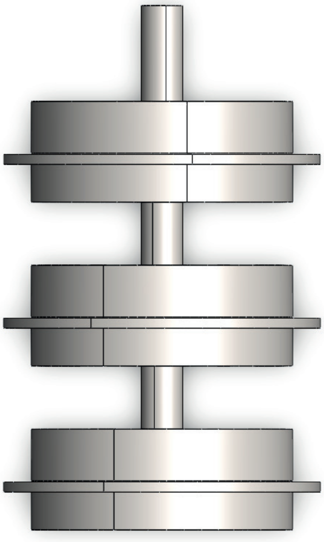

Fig. 5. Assembly of the investment-cast wheel component in SOLIDWORKS

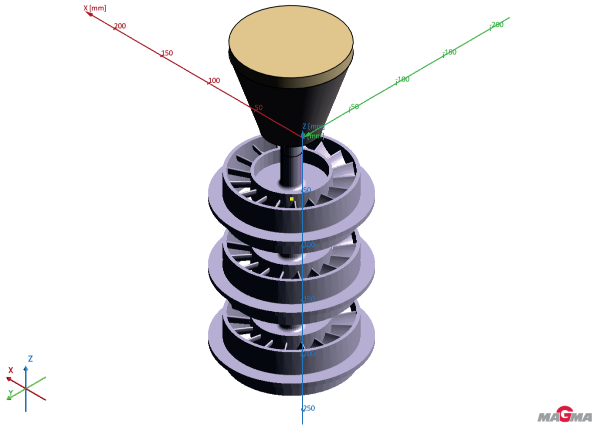

Fig. 6. Pouring basin and hot-topping geometry generated in the MAGMASOFT® geometry module

2.2. Mesh generation

Accurately predicting hot spot and porosity formation requires a fine mesh resolution in thin-walled regions. MAGMASOFT®'s advanced meshing tool was used to apply local refinement to the wheel blades and hub while maintaining coarser elements in non-critical regions. The Finite Volume Method (FVM) is used for calculations in MAGMASOFT®. A shell thickness of 10 mm is automatically generated around the casting and gating system components in mesh generation. The casting was meshed using the advanced module, while the gating system used the standard module (Fig. 7). The characteristics of the generated mesh for the initial configuration are summarised in Table 2. This ensured a good-quality mesh suitable for casting numerical simulation.

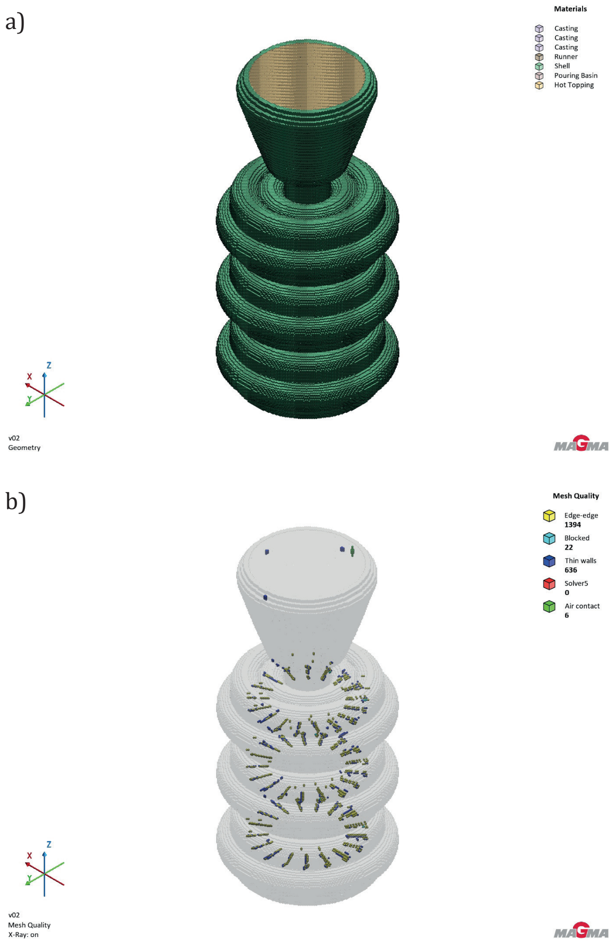

Fig. 7. Mesh generated for the casting, gating system, and ceramic shell in MAGMASOFT®: a) overall mesh distribution showing refinement in thin-walled regions of the wheel; b) detailed view highlighting element density and mesh quality in critical areas

Table 2
Mesh elements of initial design

Edge-to-edge elements	1394
Thin-wall elements	636
Blocked elements	22
Solver-critical elements	0
Air contact elements	6

2.3. Material definitions and boundary conditions

The casting alloy selected for the study was IN713, a nickel-based superalloy commonly used in high-temperature rotating components. The ceramic shell was modelled using the standard shell alumina high density material available in MAGMASOFT® database, with constant heat transfer coefficients applied at the metal-mould interface (Table 3).

Table 3
Simulation parameters considered

Alloy pouring temperature	1450–1550°C
Pouring time	Automatic filling control
Shell preheat temperature	800–1000°C
Temperature step	50°C
Feeding effectivity	50%
Sand (shell) permeability	300 cm^3/min
Hot topping initial temperature	20°C
Heat transfer coefficient (HTC)	1000 W·m^{-2}·K^{-1}

A shell permeability of 300 cm^3/min was selected to represent the permeability conditions typical of dense alumina-based ceramic shells used in vacuum investment casting. Permeability in this range restricts gas flow through the mould wall, which is consistent with the reduced-pressure environment of vacuum processing and supports stable solidification by minimising gas entrapment. In MAGMASOFT®, this parameter influences the mould venting behaviour, thermal response, and porosity prediction, making it an essential input for accurately modelling vacuum investment-casting conditions.

These values were selected based on the literature to reflect near-realistic industrial conditions for investment casting of nickel superalloys [11, 14]. In particular, the selected alloy and shell temperatures correspond to casting conditions [2, 7], while the applied HTC values are consistent with the values used in the numerical simulations [14, 16].

2.4. Design of experiments (DOE) and optimisation in MAGMASOFT®

A total of 15 simulation variants were generated by combining the alloy initial temperatures with the shell initial temperatures, as summarised in Table 4.

Table 4
Temperature design of cast and shell

Design	Cast alloy – initial temperature [°C]	Shell – initial temperature [°C]
Design 1	1450.0	800.0
Design 2	1500.0	800.0
Design 3	1550.0	800.0
Design 4	1450.0	850.0
Design 5	1500.0	850.0
Design 6	1550.0	850.0
Design 7	1450.0	900.0
Design 8	1500.0	900.0
Design 9	1550.0	900.0
Design 10	1450.0	950.0
Design 11	1500.0	950.0
Design 12	1550.0	950.0
Design 13	1450.0	1000.0
Design 14	1500.0	1000.0
Design 15	1550.0	1000.0

Each design was evaluated for:

- porosity distribution,
- hot spot formation,
- fraction liquid evolution,
- filling behaviour and flow of molten metal.

The primary and only objective selected was to identify and minimise the porosity in the wheel body.

2.5. Redesigned geometry

Based on the findings from the initial simulation, the casting geometry was modified to improve the feeding behaviour, melt flow, and overall solidification performance. The redesign included the following changes:

- The wheel component was reshaped according to the predicted hotspot and porosity regions. A draft angle of approximately 13° was introduced and applied through a geometric extrusion in SOLIDWORKS, resulting in a more favourable solidification profile (Fig. 8).
- The runner length was increased by approximately 25% to compensate for shellthickness effects during meshing and to promote more uniform metal flow into the mould cavity (Fig. 9).
- An additional wheel was incorporated into the casting tree to increase the thermal mass of the assembly. This modification was intended to alter the solidification sequence and enhance the feeding conditions by slowing the overall cooling rate (Fig. 9).
- A new pouring basin and hottopping configuration were created using the MAGMASOFT® Geometry Module to improve melt delivery and feeding efficiency during the final stages of solidification (Fig. 10).

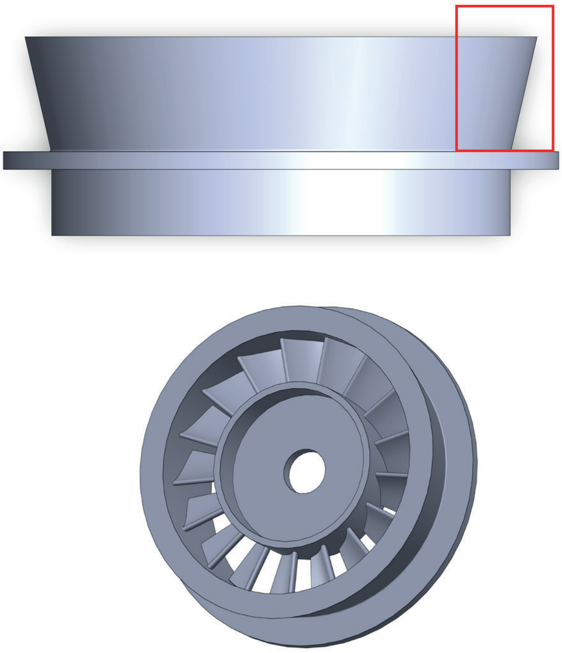

Fig. 8. Redesigned wheel geometry developed in SOLIDWORKS incorporating modifications based on initial porosity analysis

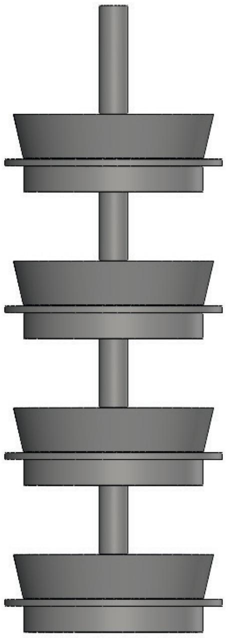

Fig. 9. Redesigned wheel geometry developed in SOLIDWORKS: assembly view showing the revised configuration of an additional wheel and extended runner prepared for numerical simulation

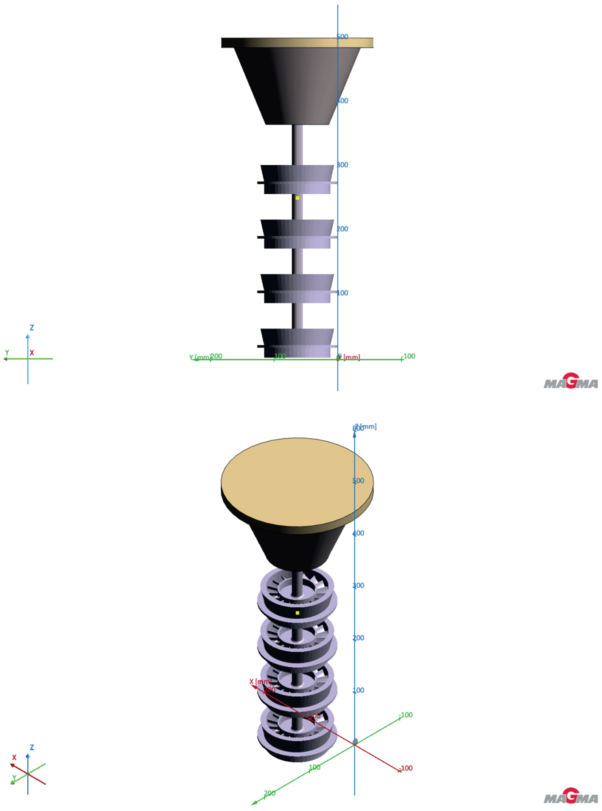

Fig. 10. Redesigned pouring basin and hot-topping configuration generated in the MAGMASOFT® Geometry Module

The redesigned model was subsequently meshed using the same refinement strategy as the baseline configuration, ensuring consistent numerical resolution across all simulations (Fig. 11). The mesh characteristics of the redesigned configuration are summarised in Table 5.

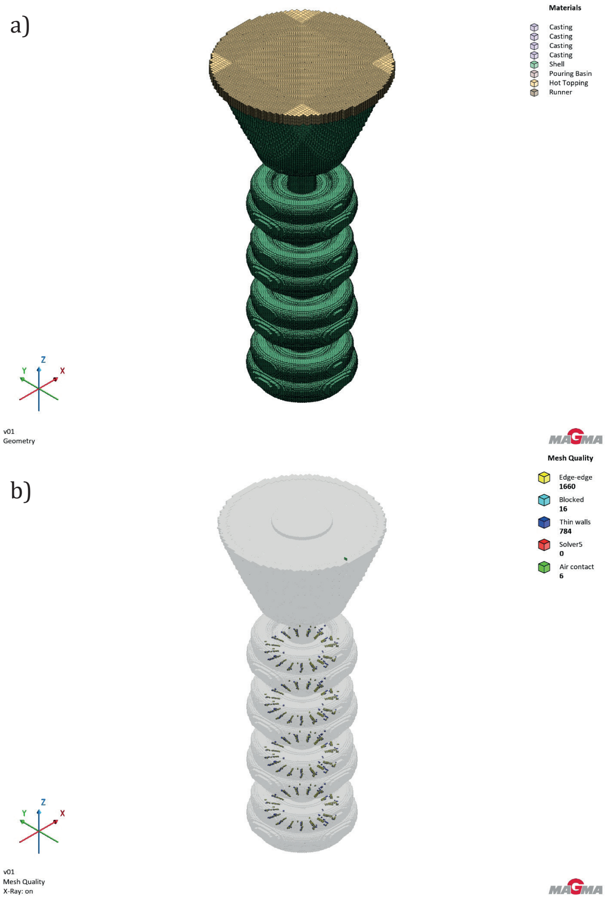

Fig. 11. Mesh generated for the redesigned casting and gating system: a) global mesh layout; b) refined mesh in thin-walled and critical areas

Table 5
Redesigned mesh elements

Edge-to-edge elements	1660
Thin-wall elements	784
Blocked elements	16
Solver-critical elements	0
Air contact elements	6

The same DOE matrix of 15 thermal variants (Table 4) was applied to the redesigned geometry.

3. RESULTS

3.1. Initial simulation results

The initial set of simulations evaluated the wheel and runner configuration under fifteen combinations of alloy and shell temperatures. The results are summarised in Table 6. The values highlighted in bold indicate the lowest porosity in the initial configuration (Design 1) and the redesigned configuration (Design 4). Among these tested variants, Design 1 (alloy initial temperature is equal 1450°C and shell is equal to 800°C) exhibited the lowest overall porosity value (5.03).

Table 6
Comparison of porosity values for initial and redesigned configurations as a function of alloy and shell temperatures

Design	Cast alloy – initial temperature [°C]	Shell – initial temperature [°C]	Porosity [–], initial design	Porosity [–], redesigned
Design 1	1450.0	800.0	**5.03**	10.36
Design 2	1500.0	800.0	5.44	11.06
Design 3	1550.0	800.0	5.55	11.85
Design 4	1450.0	850.0	5.34	**10.35**
Design 5	1500.0	850.0	5.38	11.35
Design 6	1550.0	850.0	5.52	12.22
Design 7	1450.0	900.0	5.13	10.56
Design 8	1500.0	900.0	5.50	11.46
Design 9	1550.0	900.0	5.53	12.27
Design 10	1450.0	950.0	5.16	10.76
Design 11	1500.0	950.0	5.22	11.72
Design 12	1550.0	950.0	5.58	12.08
Design 13	1450.0	1000.0	5.20	11.18
Design 14	1500.0	1000.0	5.23	11.65
Design 15	1550.0	1000.0	5.45	11.37

However, significant shrinkage porosity defects remained, concentrated in the central hub region, the blade–hub transition, and the upper parts of the wheel body. These regions correspond to thin-walled areas with restricted feeding paths, which increased their sensitivity to thermal gradients and solidification shrinkage. The observed porosity distribution is consistent with the dendritic solidification behaviour of IN713 described in the Introduction. Interdendritic regions are prone to shrinkage porosity due to solute segregation and delayed solidification, which promotes the formation of defects in the final stages of solidification. This behaviour could be correlated to the concentration of porosity in the hub and blade–hub transition regions.

The hot-spot simulation identified a dominant thermal concentration at the hub region and at the end of the blades, where solidification times exceeded approximately 230 s (Fig. 12). This prolonged local solidification promotes shrinkage porosity, most likely due to insufficient feeding and geometric constraints inherent to the initial design. The predicted hot-spot location corresponds closely with the porosity distribution obtained from the porosity-defect simulation (Fig. 13), confirming that the thermal mass of the wheel is not adequately balanced by the existing gating system. Together, these results indicate that the hub region requires improved feeding or modified geometry to mitigate shrinkage-related defects in subsequent design iterations.

The correlation analysis (Fig. 14) for the initial design reveals two distinct thermal influences on porosity formation. A strong positive correlation is observed between the initial alloy temperature and reduced porosity, indicating that higher pouring temperatures (1450–1550°C) promote improved feeding and reduced shrinkage defects. This trend reflects the longer liquidphase availability and enhanced fluidity of the melt at elevated temperatures, which support more effective inter-dendritic feeding during solidification. In contrast, the initial shell temperature exhibits a weak negative correlation with reduced porosity. Increasing the shell preheat temperature (800–1000°C) slightly increases the porosity, likely due to reduced thermal gradients and slower heat extraction, which diminish directional solidification and promote localised shrinkage.

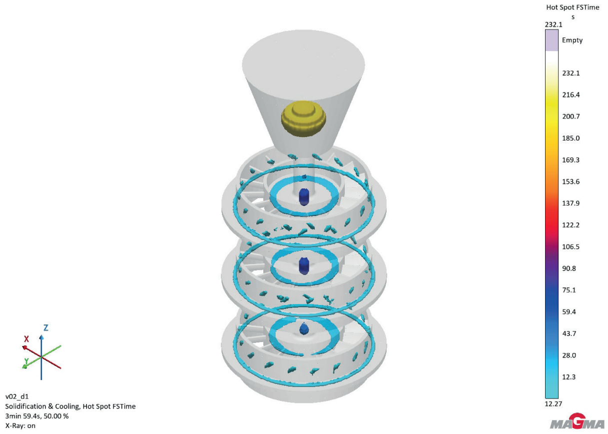

Fig. 12. Hot spot distribution for the initial design (Design 1: alloy temperature 1450°C, shell temperature 800°C)

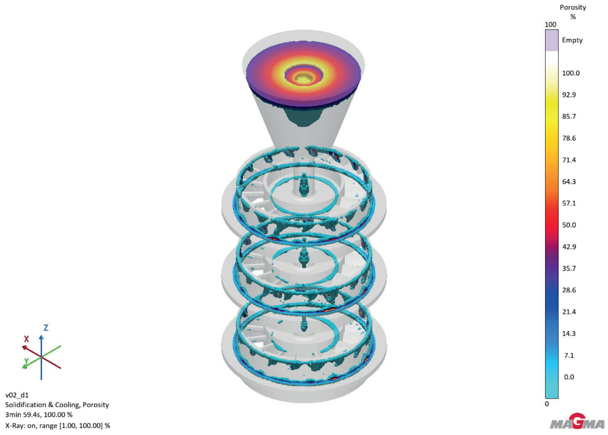

Fig. 13. Porosity distribution for the initial design (Design 1)

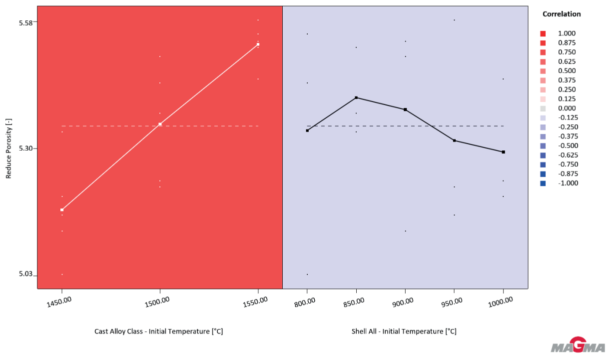

Fig. 14. Correlation of alloy and shell temperature with porosity of initial design

The pouring simulations, in contrast, revealed favourable flow conditions. Metal flow into the cavity was stable across all temperature combinations, indicating sufficient gating performance. The uniform filling suggested that the existing system could accommodate additional components on the tree, providing the idea for a redesigned geometry in the next phase of the analysis. The liquid-fraction results provided further insight into the solidification sequence (Fig. 15).

3.2. Redesigned simulation results

The redesigned configuration incorporated several geometric and gating system modifications, including a 25% longer runner, the addition of a second wheel on the casting tree, and a redesigned pouring basin with hot topping. These changes altered the thermal balance of the assembly. The extended runner improved the melt distribution towards the wheel cavity, while the additional wheel increased the overall thermal mass, slowing the cooling rate and enhancing feeding conditions during solidification.

Hot spot analysis of the redesigned configuration (Fig. 16) revealed a more uniform temperature distribution compared to the initial design, accompanied by a reduced cooling rate. The maximum solidification time increased to approximately 590 s, indicating a more controlled and progressive solidification sequence. This behaviour reflects the influence of the improved heat retention within the casting system.

The porosity distribution corresponding to the redesigned configuration (Design 4) is presented in Figure 17, with quantitative results previously summarised in Table 6. Among all simulated variants, Design 4 (alloy temperature 1450°C and shell temperature 850°C) exhibits the most favourable performance. Although the total porosity value (10.35) is higher than that of the initial configuration (5.03), a substantial reduction of porosity was achieved in critical regions, particularly in the central hub and blade-hub interface. In the redesigned configuration, porosity is predominantly located in the upper draft regions of the component, which are removed during subsequent machining operations. Therefore, despite the higher total porosity value, the redistribution of defects towards non-critical regions results in a net improvement in casting quality and structural integrity.

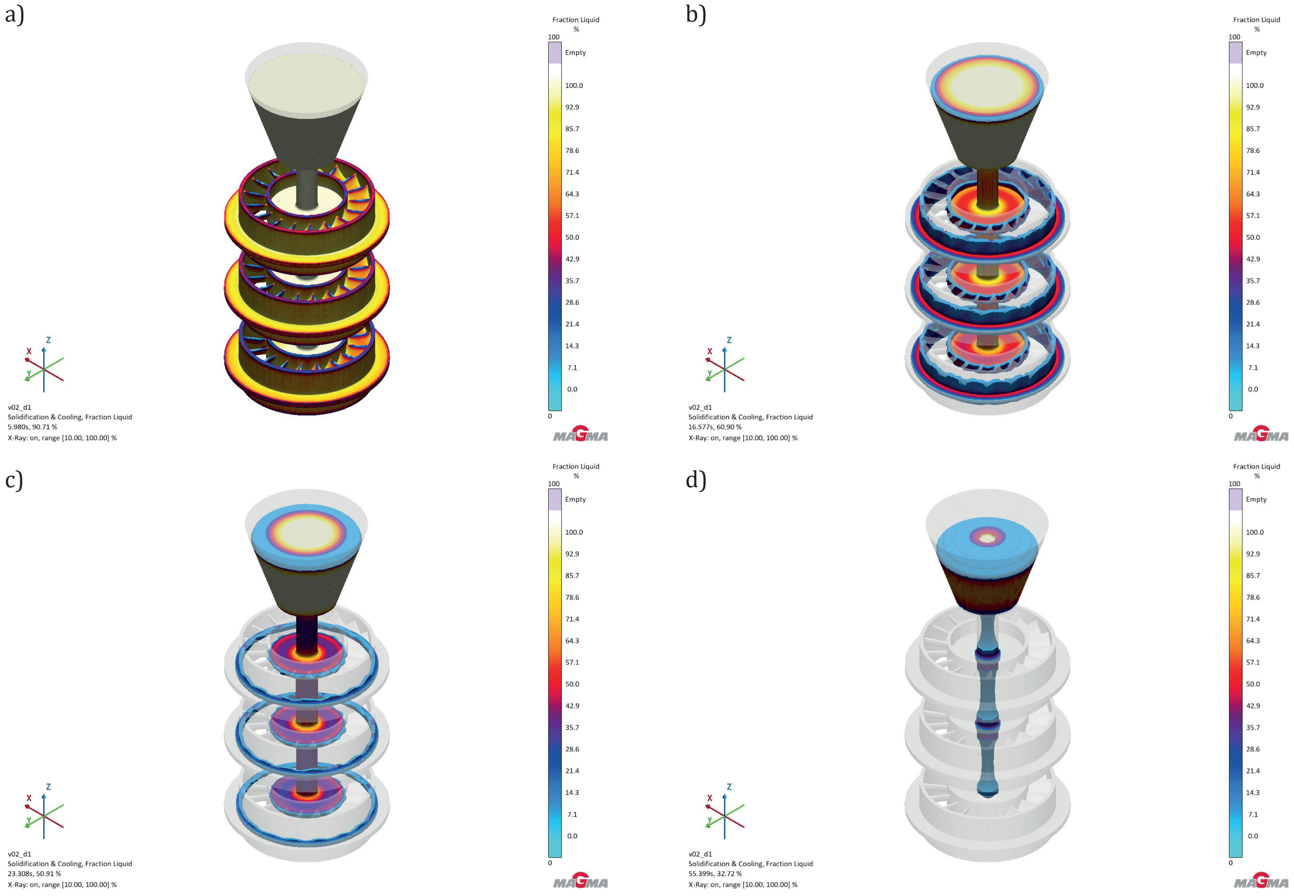

Fig. 15. Solidification stages of initial design – liquid fraction: a) 90.71%; b) 60.90%; c) 50.91%; d) 32.72%

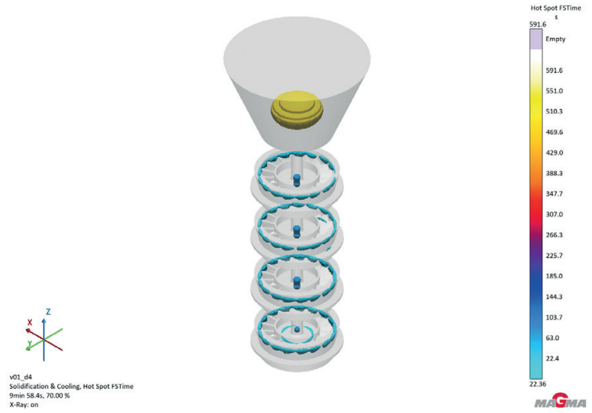

Fig. 16. Hot spot distribution for the redesigned configuration (Design 4: alloy temperature 1450°C, shell temperature 850°C)

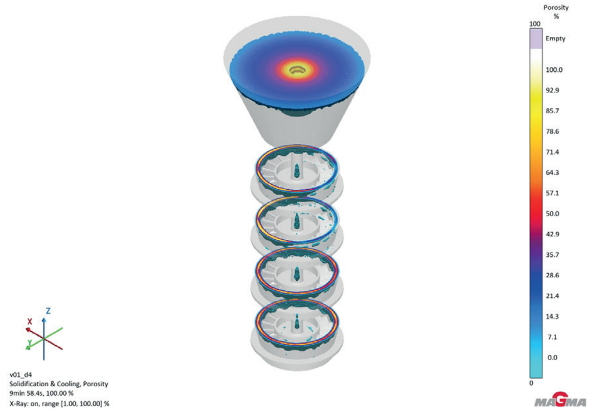

Fig. 17. Porosity distribution for the redesigned configuration (Design 4)

Correlation trends between process parameters and porosity are shown in Figure 18. Similar to the initial design, alloy superheat exhibited a strong positive influence on porosity formation, whereas shell preheating showed a weak negative influence. However, the redesigned gating system reduced the sensitivity of porosity formation to variations in shell temperature, making the alloy temperature the dominant controlling factor.

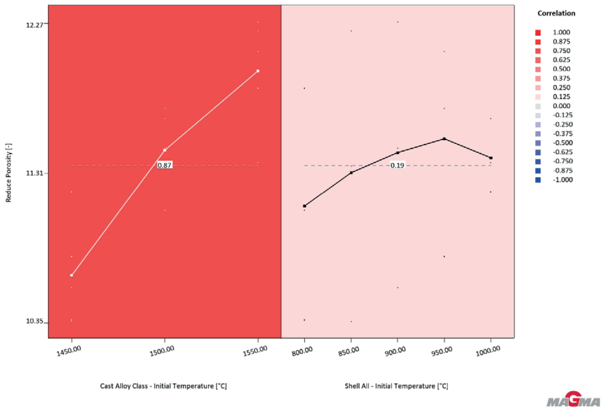

Fig. 18. Correlation of alloy and shell temperature with porosity of redesign

Further insight into the solidification behaviour is provided by the fraction liquid maps (Fig. 19), which demonstrate smoother solidification fronts and a more homogeneous temperature distribution throughout the process. The selected parameters (alloy temperature of 1450°C and shell temperature of 850°C) provided sufficient superheat to ensure complete mould filling while preventing premature solidification in thin-walled sections.

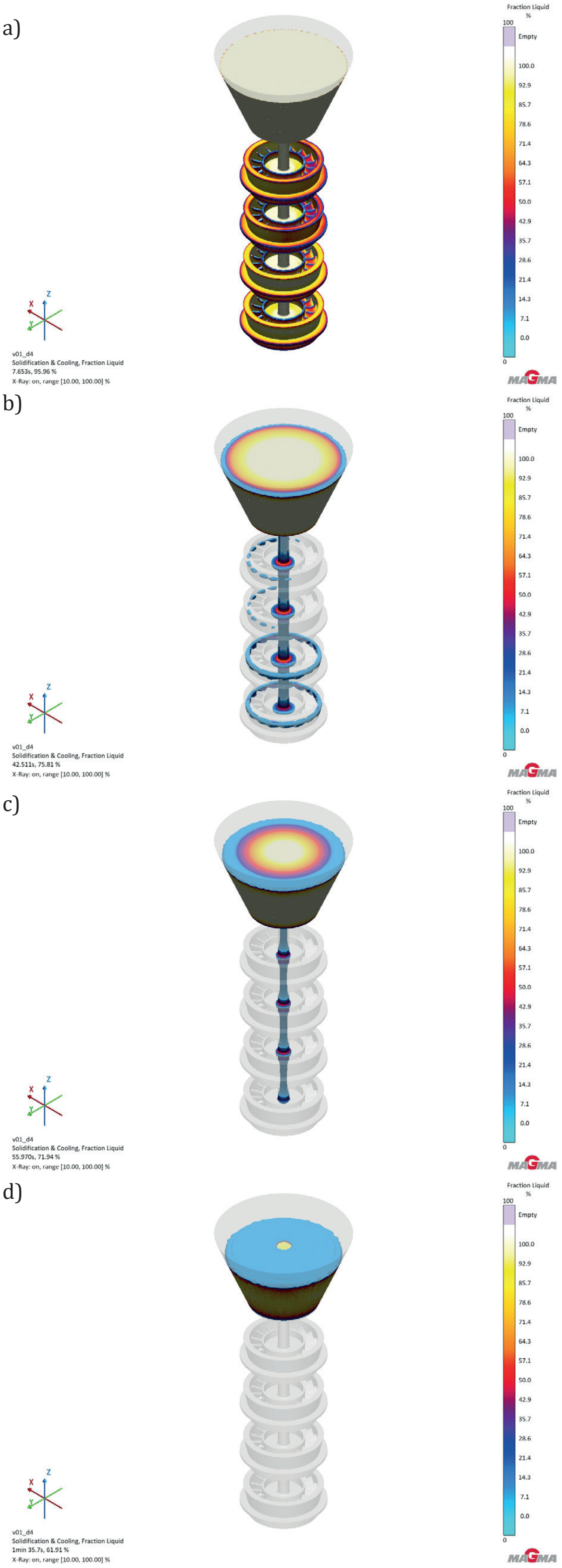

Fig. 19. Solidification stages of redesigned configuration – liquid fraction: a) 95.96%; b) 75.81%; c) 71.94%; d) 61.91%

3.3. Comparative analysis: Initial vs. redesigned

A comparison between the initial configuration (Design 1, Fig. 20) and the redesigned configuration (Design 4, Fig. 21) clearly demonstrates the benefits of the redesign. The porosity previously concentrated at the hub was significantly reduced, and shrinkage in the blade region decreased correspondingly. Although both designs maintained good filling behaviour, the redesigned configuration exhibited markedly superior feeding efficiency due to its extended solidification time and balanced thermal distribution.

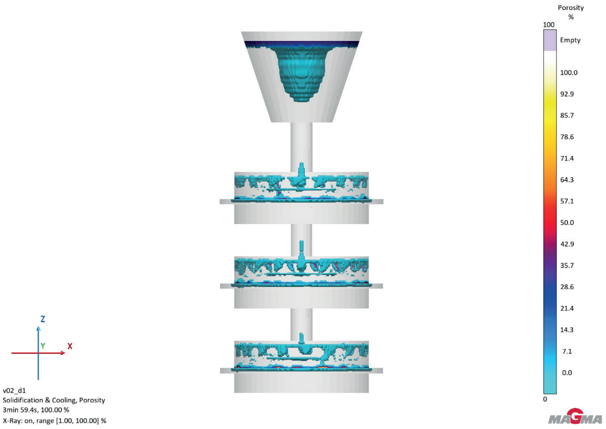

Fig. 20. Porosity distribution for the initial design (Design 1)

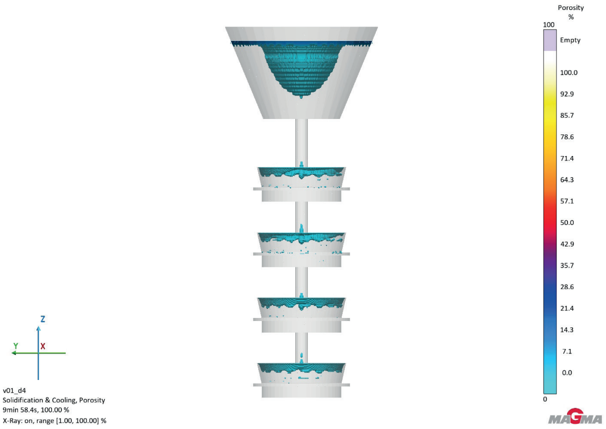

Fig. 21. Porosity distribution for the redesign (Design 4)

The hot spot duration increased from approximately 3 min 59 s in the baseline design to nearly 9 min 58 s in the optimised model, providing sufficient time for feeding and thus reducing porosity formation. Overall, the results confirm that the redesigned configuration achieved improved metallurgical soundness and thermal stability. The redesigned configuration (Design 4) effectively meets the casting quality requirements and can be further machined to restore the original geometry specifications.

4. CONCLUSIONS

The numerical simulations performed in this study demonstrated that both thermal parameters and casting system design significantly influence porosity formation in investment casting IN713 components.

In the initial configuration, the lowest porosity value (5.03) was obtained for Design 1 (1450°C alloy, 800°C shell). However, this porosity was concentrated in critical regions, particularly in the central hub and blade–hub interface, which negatively affects the structural integrity of the component.

The redesigned configuration, incorporating modifications to the runner geometry, casting tree, and pouring system, resulted in improved feeding conditions and a more favourable solidification pattern. The optimal variant was identified as Design 4 (1450°C alloy, 850°C shell), which achieved a significant porosity reduction in critical regions. Although the total porosity increased to 10.35, the defects were redistributed to non-functional regions removed during machining, resulting in improved effective casting quality.

The redesign increased the solidification time and promoted more uniform thermal gradients, enhancing feeding efficiency and reducing shrinkage porosity in critical areas. These results confirm that simulation-driven design modification is an effective approach for improving the quality and reliability of investment-cast components. The study demonstrates that optimisation of both thermal parameters and casting geometry is essential for controlling porosity formation and achieving high-quality castings for drone applications.

ACKNOWLEDGEMENTS

The work was carried out within the Erasmus+ exchange program at the AGH University of Krakow. The author would like to express their sincere gratitude to Dr hab. inż. Janusz Lelito, prof. AGH and Prof. Dr hab. Halina Krawiec of the AGH University of Krakow for accepting him into their research project and for providing access to unpublished research results.

Special thanks are extended to Prof. Dr.-Ing. Michał Szucki for his guidance and support during the specialisation in Foundry Technology and for his continued assistance.

The author would also like to thank his colleagues from the Faculty of Foundry Engineering at the AGH University of Krakow for their valuable support and insightful discussions.

REFERENCES

[1] Green Spikesley E. (1979). Investment casting. *International Journal of Materials in Engineering Applications*, 1(6), 328–334.

[2] Sjöberg G. (2010). Casting superalloys for structural applications. In: E.A. Loria (Ed.), *Superalloy 718 and Derivatives* (pp. 116–130). Warrendale: The Minerals, Metals & Materials Society.

[3] Stefanescu D.M. (2015). *Science and Engineering of Casting Solidification*. Cham: Springer.

[4] Sims C.T. (1966). A contemporary view of nickel base superalloys. *Journal of the Minerals, Metals & Materials Society*, 18(10), 1119–1130.

[5] Zýka J., Andršová I., Podhorná B. & Hrbáček K. (2014). Mechanical properties and microstructure of IN738LC nickel superalloy castings. *Materials Science Forum*, Vol. 782, 437–440. Stafa Zurich: Trans Tech Publications. DOI: https://doi.org/10.4028/www.scientific.net/MSF.782.437.

[6] Moreira M.F., Fantin L.B., Beneduce Neto F. & Azevedo C.R.F. (2021). Microstructural and mechanical characterization of as cast nickelbased superalloy IN 713C. *International Journal of Metalcasting*, 15(4), 1129–1148. DOI: https://doi.org/10.1007/s40962-020-00540-0.

[7] Rakoczy Ł., Grudzień Rakoczy M. & Cygan R. (2019). The influence of shell mold composition on the as cast macro and micro structure of thin walled IN713C superalloy castings. *Journal of Materials Engineering and Performance*, 28(7), 3974–3985. DOI: https://doi.org/10.1007/s11665-019-04098-9.

[8] Varfolomeev M.S. & Shcherbakova G.I. (2021). Interaction of a ceramic casting mold material of the Al_2O_3–Al_2O_3 composition with a nickel-based superalloy. *International Journal of Metalcasting*, 15(4), 1309–1316. DOI: https://doi.org/10.1007/s40962-020-00557-5.

[9] Dave I.B. & Kaila V.N. (2014). Optimization of ceramic shell mold materials in investment casting. *International Journal of Research in Engineering and Technology*, 3(10), 30–33. DOI: https://doi.org/10.15623/ijret.2014.0310005.

[10] Banks J. (2000). Introduction to simulation. *Proceedings of the Winter Simulation Conference*, December 10–13, Orlando, USA (pp. 9–16). Piscataway: IEEE.

[11] Campbell J. (2015). *Complete Casting Handbook: Metal Casting Processes, Metallurgy, Techniques and Design*. Oxford: Butterworth Heinemann.

[12] Socha L., Gryc K., Sviželová J., Chmiel M., Brathová M. & Filipek S. (2022). Prediction of defects of ductile iron casting by numerical simulation. *IOP Conference Series: Materials Science and Engineering*, 1243(1), 012008. DOI: https://doi.org/10.1088/1757-899X/1243/1/012008.

[13] Khan M.A.A. & Sheikh A.K. (2018). Mechanical characterization and quality of iron castings using optimized mold design: simulations and experimental validation. *The International Journal of Advanced Manufacturing Technology*, 98(1), 799–809. DOI: https://doi.org/10.1007/s00170-018-2325-y.

[14] Sabau A.S. (2005). Numerical simulation of the investment casting process. *Transactions of American Foundry Society*, 113, 407–417.

[15] MAGMA Gießereitechnologie GmbH. (2026). *MAGMASOFT®: Investment Casting Module*. Aachen: MAGMA Gießereitechnologie GmbH.

[16] Incropera F.P., DeWitt D.P., Bergman T.L. & Lavine A.S. (1996). *Fundamentals of Heat and Mass Transfer*. New York: Wiley.